# When the glacier left the volcano: Behaviour and fate of glaciovolcanic glass in different planetary environments

de Vet, S.J.

**Publication date**
2013

▲ *Wheel tracks on sol 706 when Mars rover Spirit entered the 'El Dorado' dune field in the Columbia Hills.*

# Chapter 5

## Orientation of particles to wind flow

***Abstract***

Long-axis orientation of particles in unconsolidated sediments harbours information on particle mobility in aeolian systems as it reflects the orientation to dominant wind directions. We developed a method using object-based image analysis (OBIA) to measure the orientation of sand grains. This method was first developed and validated using thin-sections of well-studied and oriented sediments in terrestrial inland dunes where it increased the available sample size, reduced operator bias and improved the analysis of grain orientation compared to pre-existing techniques. As the developed method was found to work well for terrestrial thin-sections, it was subsequently applied to images of aeolian sediments on Mars. These images were obtained using the Microscope Imager of the Mars Exploration Rover 'Spirit'. We detected non-random particle orientations in fine-grained sediments at the El Dorado and Winter Haven sites that we interpret to be caused by orientation to local winds. The flow directions inferred from these sediments seem to agree with the flow directions that formed other aeolian features in the vicinity, such as bedforms, ventifacts and wind tails. Although particle orientation occurs during saltation of particles, some degree of orientation may also reflect orientation to flow conditions below the fluid threshold. The detection of preferred long-axis orientations using the newly developed OBIA method can improve pre-existing thin-section studies of aeolian sediment on Earth and it potentially provides a new form of wind flow data that may be of interest to aeolian studies at the surface of Mars.

This chapter is based on: *De Vet, S.J., Anders, N.S., De Boer, W.M., 2013. Near-surface wind directions recorded by particle orientation in Mars' aeolian sediments (Submitted to: Journal of Geophysical Research - Planets)*

## 1. Introduction

Long-axis orientation of particles by flowing media can be used to study flow patterns. This application is well exemplified in aquatic environments where 'imbrication' is used to study turbidites (Spotts, 1964), shearing deltaic sediments (Hamilton *et al.*, 1968), costal sands (Curray, 1956) and gravelly deposits (Major, 1998). Atmospheric orientation of particles also occurs, yet it is less pronounced compared to aquatic environments (Rusnak, 1957; Schwan 1989). Inferring near-surface flow conditions from particles that have been mobilised or transported by winds is therefore infrequently applied, in spite of potential benefits to aeolian studies on Earth or surface investigations on other planetary bodies. Orientation of particles in aeolian sediments is dependent on the transport regime and as such, particle diameter. At the *static* or *fluid threshold* (Bagnold, 1954) several transport regimes can be identified depending on particle diameter. These regimes cover suspension (<20 μm), short term suspension (~20-70 μm), saltation (~70-500 μm) and reptation (>500 μm) (Kok *et al.*, 2012). A-axis orientation from long-axis streamlining of particles (Fig. 33a) occurs almost instantaneously after entrainment of ~70-500 μm grains by saltation into the turbulent boundary layer (Schwan, 1989). The resulting type of particle orientation is observed in a wide variety of aeolian sediments that vary from non-cohesive wind-blown sand deposits (Sindowksi, 1957) to lithified cross-beddings preserved in sandstones (Wayland, 1939; Schwarzacher, 1951; Martini, 1971). Other forms of particle mobility that result to preferred orientation are made possible by rolling transport at wind speeds below the fluid threshold (e.g. Nickling, 1988). Rolling traverses the long-axis (A-axis) of the particle perpendicular to the flow direction of the wind ('AB-plane' orientation, Fig. 33b). Similar AB-plane orientations may result from individual particles rolling downslope which orients the rolling axis parallel to the strike of the slope (Dapples and Rominger, 1945). Grain orientation therefore harbours valuable information on the type of particle mobility and recent near-surface flow conditions (Schwan, 1989) that can be used *de facto* to reconstruct the wind directions that deposited local cover sands and dunes (De Boer, 1992, 1996).

The interaction of the atmosphere with non-cohesive sediments also leads to the formation of aeolian dunes and ripples on Mars. These processes take place in atmospheric conditions that are different compared to Earth. Present-day atmospheric pressure averages around 6 mbar and higher pressures of 10-15 mbar are only created during periods of higher obliquity (Kieffer and Zent, 1992; Laskar *et al.*, 2004; Phillips *et al.*, 2011). The small amounts of wind speed data in the boundary layer, obtained using meteorological instrumentation on surface landers (Hess *et al.*, 1977; Sutton *et al.* 1978; Schofield *et al.*, 1997; Magalhães *et al.*, 1999; Holstein-Rathlou *et al.*, 2010) and estimates from global atmospheric circulation models (e.g. Haberle *et al.*, 1999; Michaels and Rafkin, 2008) both show that winds in excess of 10 m $s^{-1}$ are very rare. In spite of low atmospheric pressures and infrequent threshold wind speeds, sand mobility is observed to be common (e.g. Sullivan *et al.*, 2005, 2008; Fenton 2006; Bourke *et al.*, 2008, 2010; Silvestro *et al.*, 2011; Chojnacki *et al.*, 2011). Evidence for saltation of sand in aeolian systems such as dunes and ripples occurs more widely than previously assumed (Silvestro *et al.*, 2010; Hansen *et al.*, 2011; Bridges *et al.*, 2012a) and their sand fluxes are comparable to dune systems on Earth (Bridges *et al.*, 2012b). At the global scale mid-latitudinal Martian dune fields reflect unidirectional or multidirectional winds and their orientation seems to correspond to present-day atmospheric circulation (Gardin *et al.*, 2012). Since saltation is the main process driving the preferential particle orientation in aeolian sediments, observational evidence on surface processes on Mars suggest that favourable

wind conditions exist to produce these patterns in aeolian sediments on Mars. However, this assumption is debatable. The low atmospheric density may hamper, for example, airborne streamlining to produce A-axis imbrication. On the other hand, imbrication resulting from *in situ* orientation to the wind flow can potentially be more common on Mars due to the thickness of the laminar sublayer. This layer close to the surface is several times thicker than sand-sized particles, which prevents particles from being detached by saltation into the upper turbulent boundary layer (Greeley, 2002; Kok *et al.*, 2012). Combined with the well-rounded particles of Martian aeolian sediments (Sullivan *et al.*, 2008; Goetz *et al.* 2010) this boundary layer property can promote the rolling of particles across the surface. If A-axis and AB-plane orientation of sand grains from wind flow indeed occurs in surficial sediments, quantification of these sediment property provides valuable information on particle mobility in the present-day atmospheric boundary layer on Mars.

The aim of this work is to develop a method for extracting sand grain orientations from imagery and provide a proof-of-concept for determining near-surface wind flow conditions using sediments on Mars. We used *object-based image analysis* for extracting individual sand grains from imagery data and calculating particle properties such as size, length-width ratio and the orientation of the individual sand grains. The method was developed by testing it for two case studies: (i.) thin-sections made from aeolian deposits with known grain orientations from pre-existing studies in two dune fields in Southern Brandenburg (Germany); and (ii.) lander imagery of non-cohesive surficial sand deposits in the Columbia Hills on Mars.

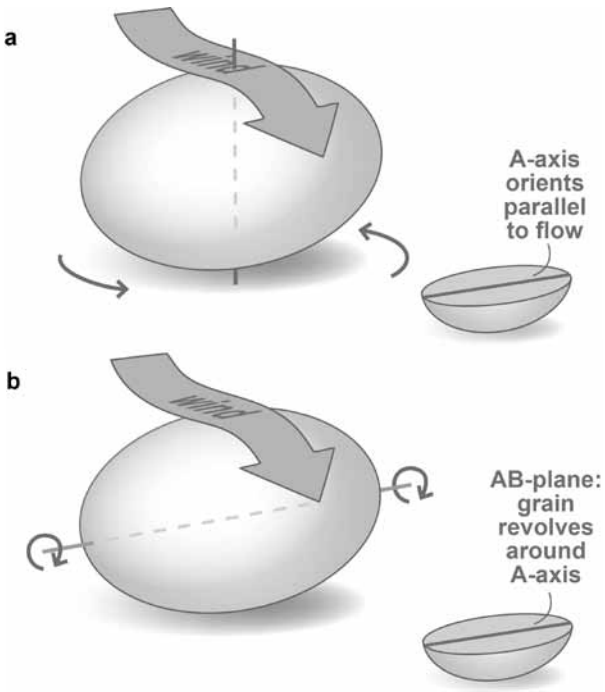


**Fig. 33** - Illustration of orientation processes that result to preferred orientations of 'imbrication' of aeolian sediments. Airborne A-axis orientation (a) occurs during saltation when an ellipsoid sand grain (here slightly exaggerated) pivots around the short axis and streamlines the long-axis (A-axis) to the local wind flow. AB-plane orientation results from rolling when the particle revolves around the A-axis, induced by either wind forces acting on the sand grain (b), or from gravity-induced rolling over an inclined surface.

## 2. Background on extracting long-axis orientation of sand grains

Methods for measuring long-axis orientation of elongated quartz grains in unconsolidated or lithified aeolian sediments have focused primarily on analysing thin-sections made parallel or perpendicular to the bedding of the sediment fabric (Martini, 1971). Using the rotation method for cross-polarised microscopy developed by Bonham and Spotts (1971), required the manual selection and the optical measurement of several hundred suitable quartz grains per thin-section. These lengthy procedures were improved using video-based processing software and hardware to count and measure a variety of grain parameters (Jenkinson, 1989). Several studies successfully used these techniques for the detection of grain orientation in thin-sections (Schwan, 1989; De Boer, 1992). However, in order to obtain sufficient contrast and image data, thin-sections needed to be viewed under polarised or cross-polarized light over 16 axes, or 'ferrets' (Fitzpatrick, 1980). More complexity is introduced in such video-based orientation measurements by the need to exclude boundary pixels in a sand grain due to irregular changes of the pixel values during the rotation under crossed polars. The applicability of this technique at a given image resolution therefore reduces drastically for smaller particle diameters. These boundary effects and the small forms of overlap between two adjacent grains at their boundaries (Heilbronner and Pauli, 1993) required small grains to be avoided in these types of measurements (Passchier and Trouw, 2005). Meanwhile, software developments of image processing tools have shown that similar results as in manual thin-section analysis methods can be obtained, with and without the use of the rotation between crossed polars, at much faster and automated rates compared to the methods used in previous studies (Heilbronner, 2000; Zaniewski, 2001; Fueten and Goodchild, 2001; Sime and Ferguson, 2003, Li *et al.*, 2008; Hassanpour, 2011).

A recent development that allows similar orientation data to be extracted from imagery of sand grains is Object-Based Image Analysis (OBIA; see Blaschke, 2010, for an extensive review). OBIA is based on the automatic clustering of image grid cells into objects or polygons (more information on OBIA is presented in section 3.1). In geosciences OBIA has been previously applied to various gridded datasets, including airborne or satellite imagery data and elevation data. In aeolian or sedimentological research thin-sections under cross-polars provide sound imagery data for OBIA analyses due to the high contrast between individual grains and the background. OBIA can therefore be applied to imagery of thin-section to isolate individual sand grains and measure long-axis orientation, as well as other sediment statistics (e.g. Urbanski *et al.*, 2011). For obvious reasons it is not possible to produce thin-sections from sediments at the Martian surface. However, the versatility of the OBIA method lends itself for application to conventional imagery of sand grains in aeolian sediments in order to measure sediment properties and infer long-axis orientations of grains on Mars. This planetary application benefits from the pre-existing cadre of well-established thin-section studies on Earth. We therefore used thin-sections of horizontally laminated sediments in terrestrial inland dune as a test bed to develop a general method to extract particle orientations.

## 3. Methods

This section is divided into three parts. The first part (3.1) describes the general procedure of sand grain extraction from imagery data and the subsequent granulometric analysis. The second part (3.2) describes the case study from the Schöbendorf and Klein Zieschte dune complexes in Southern Brandenburg (Germany). Here we validated the automated procedure with an existing and well-studied dataset of sand deposits formed by comparable

unidirectional wind flow conditions as the present-day surface winds on Mars. The third part (3.3) presents the case study where we finally applied the OBIA method to imagery data of aeolian sediments in the Columbia Hills, obtained by the Mars Exploration Rover 'Spirit'.

### *3.1 Extracting sand grain properties from imagery data*

As noted, the method on extracting sand grain properties is based on Object-Based Image Analysis (OBIA) techniques. OBIA consists of two main concepts, namely image segmentation and object classification. Image segmentation is the process of clustering grid cells into homogenous groups or 'objects', based on values of gridded data sets. These objects are subsequently categorized into classes using criteria related to; (i.) object statistics (e.g. mean, standard deviation, range) of enclosed grid cell values; (ii.) shape properties (e.g. main direction, length-width ratio, size, roundness) and/or; (iii.) topological relationships between objects or (geo)spatial context. Any type of gridded data set can be used as input for object-based analyses technique, such as aerial photography and multi/hyperspectral satellite imagery (e.g. Burnett and Blaschke, 2003; Blaschke, 2010) and digital elevation data (e.g. Van Asselen and Seijmonsbergen, 2006; Anders *et al.* 2011), or even MRI, X-Ray, and microscope images in medical disciplines.

The concept of OBIA is implemented in the commercially available software package eCognition (Trimble, 2011). The multi-resolution segmentation (MS) algorithm (Baatz and Schape, 2000) is a widely-used region-growing algorithm to formulate homogeneous objects based on 'colour' values (i.e. grid cell values). The algorithm allows the definition of a shape parameter (a dimensionless value ranging from 0-1) to prevent generating very irregularly

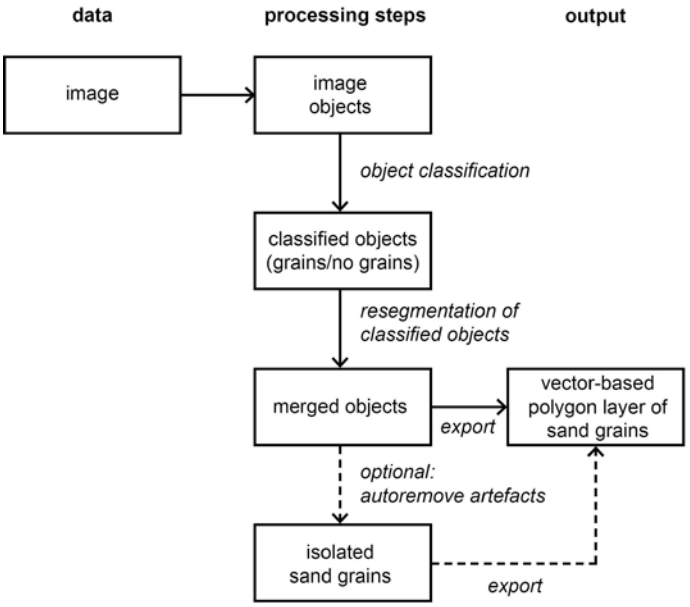


**Fig. 34** - Work flow of the object-based image analysis strategy. The flow is divided into three phases where (i.) objects are obtained by segmentation of the original image, (ii.) subsequent object classification and reclassification leads to the identification of individual sand grains that are then (iii.) exported as polygons with an appended attribute table that contains their features such as surface area, length-width ratio and orientation of the long-axis. Fig. 37 shows a visual reference of the three consecutive steps.

shaped objects. When a higher shape parameter is defined (close to 1), less weight is assigned to colour values in the process of object delineation. In this research presented here the shape parameter was set to an average value of 0.5 to prevent the generation of very irregularly shaped objects, but allow colour values to drive the general object shape. The additional scale parameter in the algorithm influences the size of the objects and is closely related to the image quality (blurred images require smaller scale parameters for equally sized objects) and spatial resolution (images with smaller grid cells require larger scale parameter values for equally sized objects). The scale parameter was iteratively determined to obtain the most optimal value to accurately enclose individual sand grains in the image. Once segmented, sand grains were classified to differentiate between foreground elements (sand grains) and background noise (i.e. organics, interparticle pore spaces and dust). The actual procedure used for the processing of thin-section imagery and Mars rover imagery data, as depicted in Figure 34, was as follows:

1. **Image segmentation** to create small objects. The individual grains are oversegmented (one grain consists of multiple objects) to prevent oversized objects where grains are mixed with background noise. Depending on the quality of the imagery data the first step was preceded by an edge-preserving median filter with a 3x3 moving window (kernel) to enhance the contrast of the image (this was essential for the imagery data of surficial sediments on Mars).
2. **Classification of objects** to differentiate between sand grains and background noise.
3. **Resegmentation of objects** that were classified as 'sand grain' with a larger scale parameter value to merge the oversegmented objects. After this step individual objects represent entire sand grains.
4. **Removal of segmentation artefacts** by excluding objects with a roundness larger than 1.2.
5. **Exportation of objects** classified as 'sand grains' as polygons to a vector-based shape file with an appended attribute table containing polygon properties (e.g. area, length, width) that were automatically calculated by eCognition. This vector-layer formed the basis of the subsequent orientation and granulometric analyses.

The processing steps and their corresponding parameter values are summarised in Table 6. All thin-section data could be processed with a single rule set. The Martian surficial deposits images used the same extraction strategy, but with different parameter settings due to different spectral conditions of the images (more information on this matter is found in the following subsections). Individual shape properties were determined for each of the polygons representing extracted sand grains and included the main orientation direction, length-width, and surface area. Length-width ratios were computed due to the effect of different ratios on the calculated degree of imbrication and its use to select a suitable sample subset to infer the wind flow directions from the sediment fabric. Schwan (1989) defined a set of suitable parameters for describing the long-axis orientation of aeolian sediments. The most notable is the mean resultant length ($R$) as a measure for the overall fabric strength. This parameter is a relative value between 0 and 1 for the concentration (variation) around the mean orientation of the sediment fabric and it is calculated for eighteen 10° intervals using:

$$R = \{(C/n)^2 + (S/n)^2\}^{0.5} \text{ , with } C = \sum_{i=1}^{18} f_i \cdot \cos 2\alpha_i \text{ , } S = \sum_{i=1}^{18} f_i \cdot \sin 2\alpha_i$$

Here, $n$ is the total amount of measured sand grains, $f_i$ the amount of grains per interval and $\alpha_i$ the mid-class point of the interval (with $\alpha_i$ = 5°, 15°, 25°, …, 175°). As the preferred

**Table 6** - Process parameters used in the object-based image analysis (OBIA) strategy. Images were analysed using the commercially available software eCognition, according to the workflow in Fig. 34 with the use of the set of parameters specified below.

| Process | Parameter | Brandenburg | Mars | | |
|---|---|---|---|---|---|
| | | | *Shadow* | *King George Isl.* | *Troll* |
| Median filter | - | - | 3 | 3 | 3 |
| Segmentation | Layer | RGB | median | median | median |
| | Scale | 20 | 10 | 10 | 35 |
| | Shape | 0.5 | 0.5 | 0.5 | 0.5 |
| Classification | Mean Red | > 120 | - | - | - |
| | Mean median value | - | > 300 | > 1200 | > 1200 |
| | Roundness | > 1.5 | > 1.15 | > 1.15 | > 1.15 |
| | Length/width | - | < 1.6 | < 1.6 | < 1.6 |
| | Area | - | - | - | < 250 |
| Segmentation | Layer | RGB | median | median | median |
| | Scale | 80 | 25 | 25 | 50 |
| | Shape | 0.5 | 0.5 | 0.5 | 0.5 |
| Remove artefacts | Roundness | > 1.2 | - | - | - |

orientations of grains is measured in a 2D plane, the long-axis orientations is strictly non-vectorial such that inferred directions are either in $x°$ or $x°+180°$. The mean of the preferred orientation direction of grains ($x$) is then defined by:

$$x = 0.5 \cdot \tan^{-1}(S/C) + K \cdot 90°\text{, with } K = 0, 1 \text{ or } 2$$

Here, $K$ is a value used to calculate the preferred orientation per quadrant due to the asymptotes occurring every 90° in a tangential function. In addition to parameters for describing the preferred long-axis orientation, object properties such as the particle surface area were used to calculate more general sediment properties such as particle diameter distribution (Urbanski *et al.*, 2011).

### *3.2 Case study 1: Thin-sections of Schöbendorf and Klein Ziescht, Germany*

The thin-sections used in this study were made from laminated aeolian sediments exposed in the sandpits near the village of Schöbendorf and a comparable depost at Klein Ziescht (see Fig. 35). The area is located in the Central Glogów (Glogau)-Baruth ice-marginal valley. The Baruth valley was the main discharge channel that drained the meltwater of the Brandenburg ice-margin (maximum Brandenburg advance at about 24 kyr BP, Litt *et al.* 2007 to about 20-21 kyr BP, Heine *et al.*, 2009). Schöbendorf and Klein Ziescht are located on the oldest of the river terraces that were formed by at least four consecutive discharge events (Juschus, 2001). The Baruth ice-marginal valley is part of the Brandenburg young moraine landscape ('Jungmoränenlandschaft'), which was formed during the Weichselian glacial stage when the area was devoid of vegetation. Aeolian processes were the dominant agent for mobilising and transporting cover sands and the subsequently formation of several (up to 25 m high) inland dunes, mainly in the form of longitudinal, transverse, hummocky and parabolic dunes. These dunes consist for more than 95% of sand-sized (63-630 µm), well-rounded quartz grains (De Boer, 1992) and were formed by winds from roughly westerly and southerly headings (De

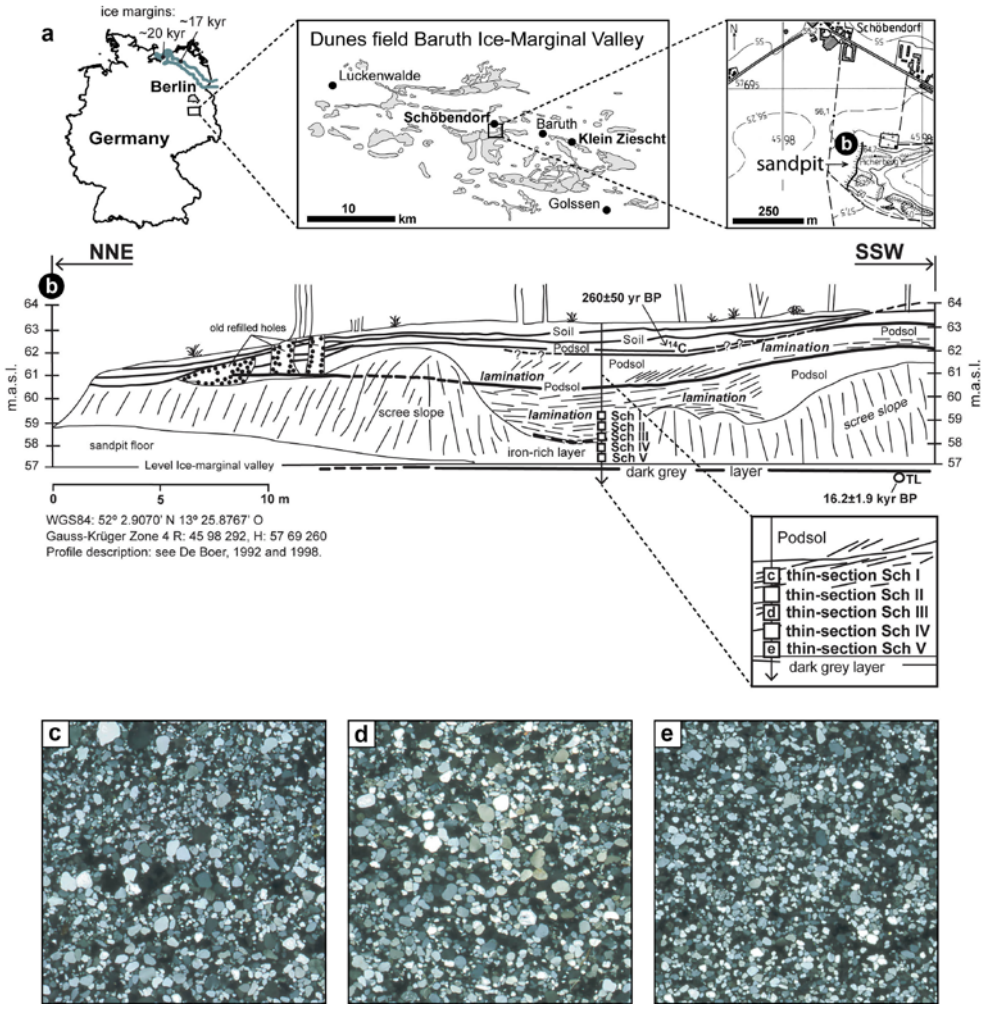


**Fig. 35** - Aeolian sediment exposed in the Picherberge quarry near Schöbendorf (a, modified from: De Boer, 1992, 1998, glacial margins are based on: Ehlers *et al.*, 2011; Brandes *et al.*, 2012). The illustration (b) shows the subsurface structure in the north-north-westerly exposure of the Picherberge complex. The geomorphological setting of the Klein Zieschtdune is nearly identical to the Schöbendorf dune and samples were obtained from similar strata. Excerpts of the thin-sections (10x10 mm) were made from undisturbed laminae and are shown here between crossed-polars (c-e). The grain morphology and the conditions of the late-Weichselian genesis of these dunes, in dry periglacial conditions devoid of vegetation, are comparable to the conditions in which well-rounded aeolian sediments are currently being transported on Mars.

Boer, 1996). The similarities in particle diameter and morphology of these sand deposits with the well-rounded sand grains in aeolian sediments on Mars (Sullivan *et al.*, 2008; Goetz *et al.*, 2010) allowed us to use these inland dunes as a test-bed to develop a strategy for application of the OBIA method to aeolian grains on Mars. The goal of the first stage in our study was therefore to demonstrate the effectiveness of the OBIA method within a small but well-studied dataset of aeolian sediments with the purpose of validating the developed method with results from pre-existing thin-section analysis techniques. We used the same thin-sections of the Schöbendorf and Klein Zieschtprofiles that were used in the study of De Boer (1992), which

were sampled roughly plane-parallel to horizontal laminae. Thin-sections were scanned with a pixel resolution of 9 μm between crossed-polarisation filters to increase the optical contrast (Fig. 35c-e).

Table 6 summarizes the OBIA processing steps and parameter values used for the processing of the thin-sections. Objects have been formed based on their Red, Green, and Blue (RGB) colour values in the original thin-section images. In this case only the red colour band was sufficient to differentiate between the sand grains and the background noise. A final step before exporting the sand grains to a polygon layer was required to remove segmentation artefacts, which have been identified based on their irregular shape. The 'roundness' property was used to automatically identify these irregularly shaped objects. Roundness is a standard property that can be derived from objects in eCognition software, and describes how well an object fits into an elliptic shape. Roundness is calculated by the difference of the outer ellipse and the inner ellipse (Trimble, 2011). Objects with a roundness value higher than 1.2 were considered irregularly shaped and were therefore removed from the final collection of classified sand grains. With the obtained polygon layer other sediment statistics such as grain size distribution can be calculated. For the purpose of comparing the OBIA method to earlier research by De Boer (1992), we have limited the analysis to comparing the frequency distributions of long-axis orientations and fabric strength properties using the methods described in section 3.1.

### *3.3 Case study 2: Surficial sands in the Columbia Hills, Mars*

Images from sand grains at the surface of Mars were obtained during the primary mission phase of the MER B, or 'Spirit' rover, using the Microscope Imager located at the end of the robotic arm (Herkenhoff *et al.*, 2003). This fixed-focus CCD camera is used for extreme close-ups of rocks and soils and has a field of view of 31x31 mm with a pixel resolution of 30 μm. Images made by the Microscope Imager (MI) are taken plane-parallel to the surface to obtain a consistent focus across the image. The projected surface of the grain therefore reflects the morphology of axes that have oriented to the local wind flow. Particles with a minimum surface area of 20 pixels contain sufficient object data for segmentation with eCognition, which means that grain orientation in Martian sediments can be detected to a lower size limit of 100-150 μm. This detection limit is well in line with the sand-sized particle diameters that are regularly mobilised by aeolian processes and the estimated particle sizes of aeolian sediments in the Columbia Hills (Sullivan *et al.*, 2008; Kok *et al.*, 2012). By multiplying or 'rotating' the state vector (1 0 0) with the quaternion of each image (a vector composed of 4 complex numbers for describing orientations and motion in a 3D space) we obtained the pointing vectors of the camera, which were then decomposed into an azimuth and elevation to determine grain orientations relative to true north. Due to the shallow 6 mm deep focus, the camera had to be positioned plane-parallel to the imaged surface. The calculated tilt of the image plane could therefore be used to determine if the slope angle of the deposit has been favourable for rolling and as such particle orientation parallel to the strike of the slope (Land, 1964; Rees, 1968). Other preferred orientations were therefore interpreted the primary orientation axis that reflects the local wind flow direction.

Suitable images of undisturbed sediments were obtained on sol 707, 1034 and 1085 during Spirit's traverse of the Columbia Hills (a 'sol' is the mission's Martian day number starting at landing). Other studies have extensively explored the sand-mobility in this area and inferred the local wind flow patterns from aeolian features such as bedforms, ventifacts, wind tails and

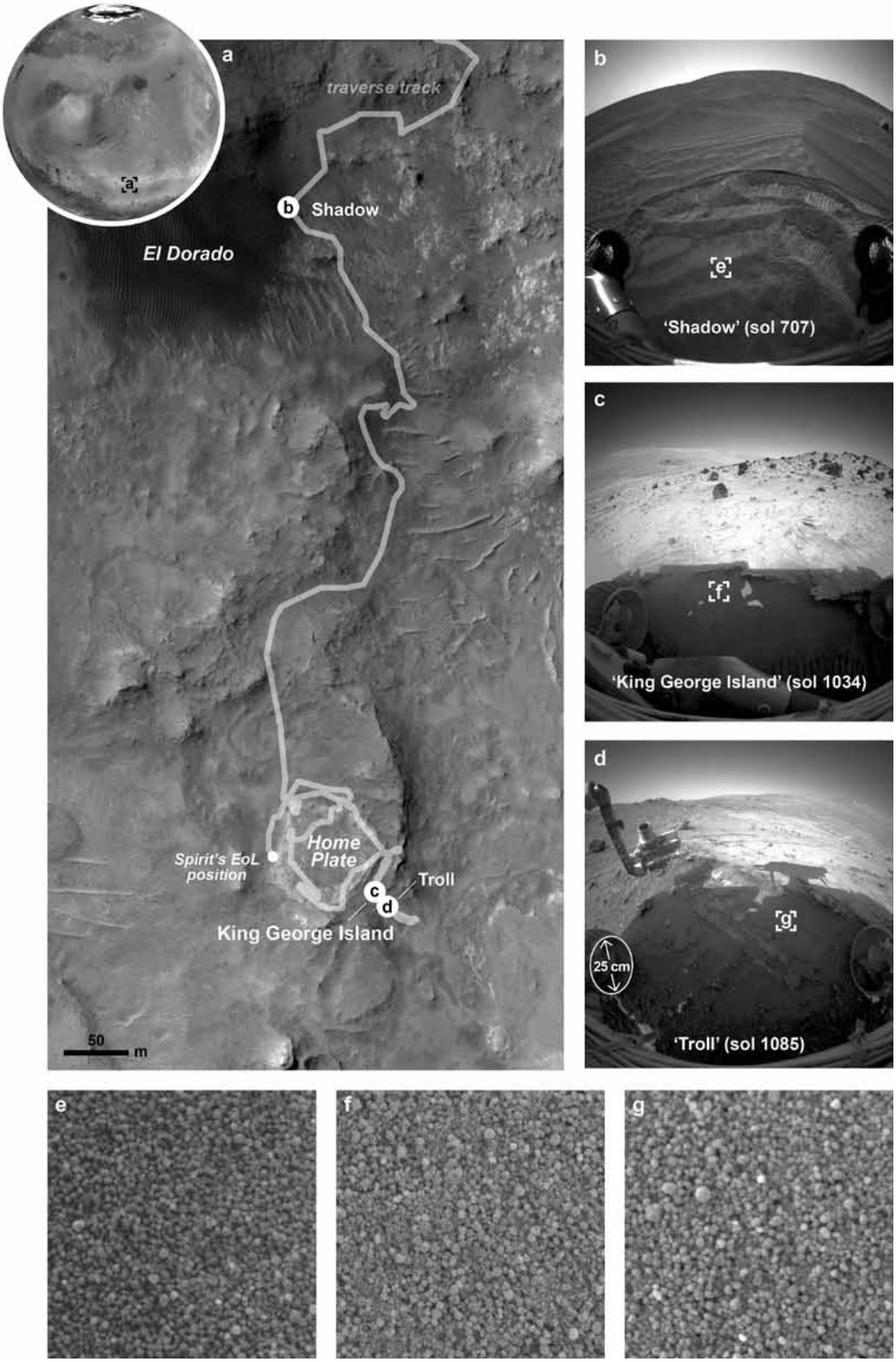
a
traverse track
b Shadow
El Dorado
Home Plate
Spirit's EoL position
Troll
c
d
King George Island
50 m
b
'Shadow' (sol 707)
c
'King George Island' (sol 1034)
d
25 cm
'Troll' (sol 1085)
e
f
g

dust streaks (Greeley *et al.*, 2008; Sullivan *et al.*, 2008; Thomson *et al.*, 2008). This provides a well-documented setting for understanding and explaining preferred orientations observed in the used imagery. The selected locations at the El Dorado dune field and two sand deposits SE of Home Plate are composed of similar-sized, well-rounded mafic sand grains free from interstitial dust (Fig. 36). Overlapping images of sands at the 'King George Island' (KGI) target at the Winter Haven site (Fig. 36c) were first used to establish if the developed technique would give the same result for images of the same grains but with different pointing vectors of the camera. The segmentation strategy was then applied to a comparable sand drift located a few meters away at 'Troll' (Fig. 36d). As both sites are impeded sand drifts pinned down between the same resistant platy layers (Arvidson *et al.*, 2008), the comparable flow conditions over these two sites are ideal for detecting and discriminating between A-axis orientation from saltation and possible AB-plane orientation from rolling of particles down-slope. Finally, orientations of particles in the 'Shadow' ripple at El Dorado served as an independent site to study preferred particle orientations and flow directions in an area with a topographically more complicated bed.

A similar OBIA procedure as for the thin-sections was applied to the images of the Martian aeolian sands, though with different parameter values. Table 6 summarises the used rule set and parameter values for the images in the three locations. Due to high ISO noise in some areas in the images a median filter was required to enhance the suitability of the images for segmentation. The edge-preserving median filter with a 3x3 moving window (kernel) slightly blurred the images and removed the high ISO noise in the image. This allowed a more accurate delineation of individual sand grains. The digital colour or brightness value differed notably between the images due to different light conditions during surface imaging operations (the 'Shadow' area was imaged in deep shade, in contrast to highly exposed images at the King George Island and Troll targets. The quality of the images also influences the scale parameter values; the image in the Troll area being slightly sharper than the other areas. Similar to the processing of the thin-sections, digital representations of the sand grains were exported to a vector-based polygon layer to calculate granulometric properties such as length-width ratio, surface area, and orientation. The detected orientations in the sediment fabric were then compared to local hillslope angles and wind directions that were inferred from local aeolian features such as dunes, ripples and ventifacts along the traverse of the Colombia Hills (Greeley *et al.*, 2008; Thomson *et al.*, 2008) to understand the contextual relation of the three studied sites with the local flow patterns.

## 4. Results

### *4.1 Thin-sections of Schöbendorf and Klein Ziescht*

The increased contrast from thin-sections under crossed-polars made the segmentation of the imagery straight forward as grains are easily separated from dark background in the image (Fig. 37). The excerpt of the original image and the classification results (Fig. 37) illustrated that a large quantity of sand grains with different particle diameters can be classified using this method for thin-section analysis ($n_{tot}$ in Table 7). Based on the calculated length-width

**Fig. 36** (left) - Traverse map of the Spirit rover in the Columbia Hills, spanning from the El Dorado dune field to Home Plate (a). Locations used for the object-based image analysis include the 'Shadow' ripple located 8 m inside the El Dorado dune field (b) and two sand drifts at the 'Winter Haven' site SE of Home Plate where grains are perched on slopes below the exposed resistant lava layers at 'King George Island (c) and at the 'Troll' ridge (d). Diameter of the rover wheel is given for size. The 10x10 mm excerpts of MI imagery (e-g) show the comparable well-rounded morphologies of 100-300 μm sand grains that have no appreciable bonding to other particles in these deposits.

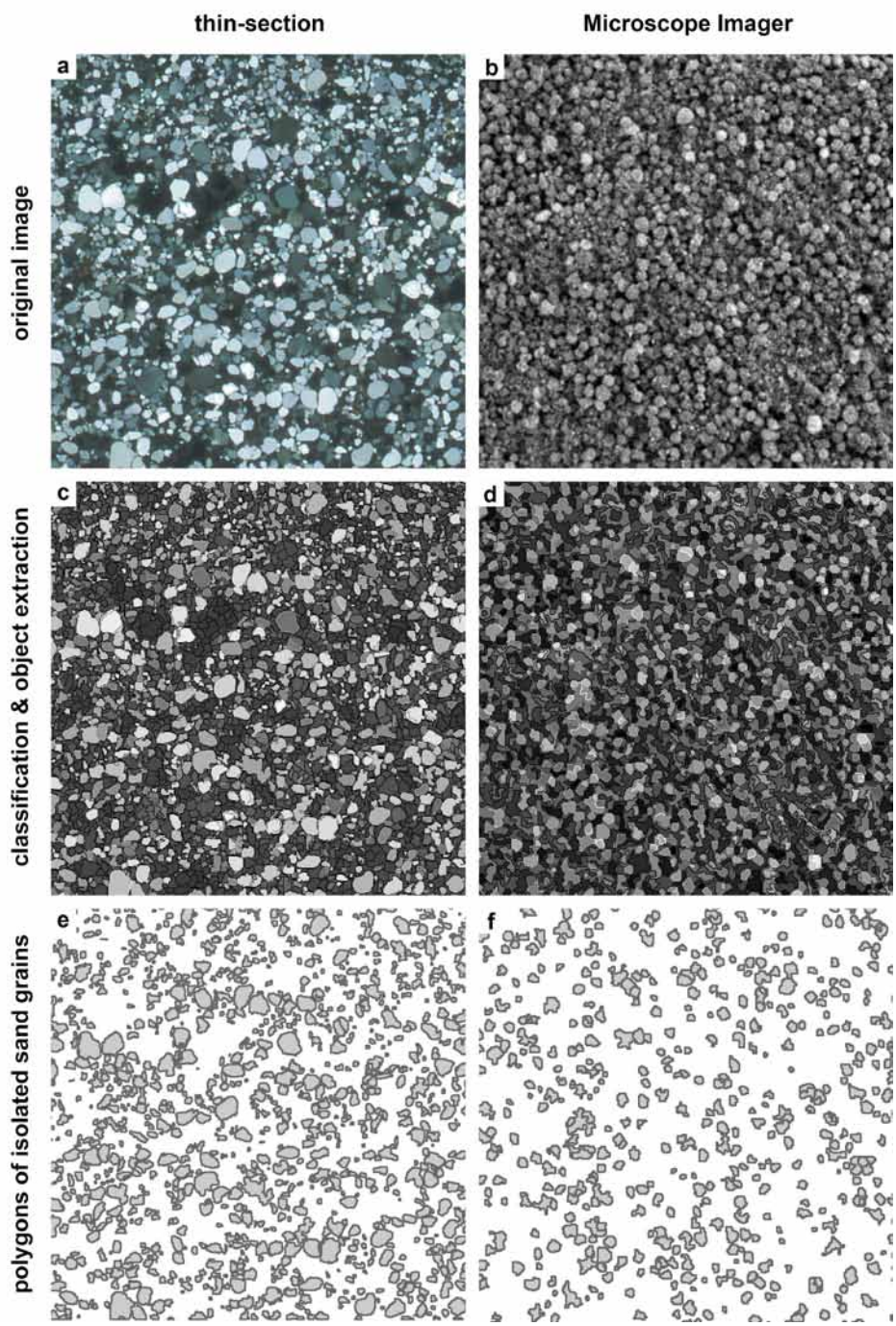


**Fig. 37** - Steps in the object-based analysis shown for 10x10 mm excerpts of the original images. Steps show how the original image (a,b) is decomposed (segmented) into polygons of similar pixel data (c,d) and classified to obtain the eventual polygons that reflect the outline of individual grains (e,f). The same strategy was used for the objected-based image analysis for thin-sections and imagery obtained by the Microscope Imager on Mars. Comparable polygons are produced and this highlights the ability of object-based image analysis to produce similar sediment statistics, independent of the type of sand-grain footage.

ratios a subset was selected containing particles with a length-width ratio of >1.5, similar to De Boer (1992). While not all grains in the thin-sections were identified based on the used rule-set (some of the darkest grains are omitted), or eventually included on the basis of their length-width ratios, the amount of grains used in the calculations is still 3-6 times more than those manually selected in pre-existing studies (compare the $n_{>1.5}$ values in Table 7). The selected subset allowed the frequency distribution of the long-axis orientations and fabric strengths to be calculated with the parameters as summarised in Table 7. Rose diagrams (Fig. 38) show bimodal headings with a preferred and a transverse heading. Average headings of the preferred orientations are illustrated in the wind roses by blue ($x$) and green lines ($x_a$) and they are compared to pre-existing measurements (in red) in Fig. 38. Preferred orientations were found to be very consistent throughout the depth of the profile (sample depths shown in upper left-hand corners of the wind roses) and they are also very comparable between the two sites. Despite the spatial separation of 7 km, both sites indicate wind directions oriented along an azimuth of (N)NE-(S)SW. These headings are in good agreement with pre-existing studies, although SCH I and SCH III show a deviation of 5-28°.

### *4.2 Surface images on Mars*

The same processing method as for the terrestrial thin-sections was used for the imagery of surficial sediments on Mars. However, low exposures, image contrast and increased ISO noise (Fig. 36e-g) required the adaptation of the process parameters in the rule-set to compensate for these differences in imagery data, which yielded comparable results as in the analysis of the thin-sections (Fig. 38 vs. 39). Obtained polygons of sand grains in the MI imagery are clearly affected by the pixel-resolution of the CCD camera (30 μm) and grains therefore generally appear jagged compared to the higher-resolution of the thin-sections (9 μm). This did not interfere with the computation of sediment statistics as the majority of particles exceeded the minimum required object size of 20 pixels, or particle diameters of 100-150 μm (Fig. 39, first column). The algorithm was first applied to the overlapping images at the drift sand of 'King George Island'. In spite of the different pointing vectors of the MI camera, orientations of grains measured in both images and their orientation relative to true north are in good agreement (Fig. 39). Processing and analysis of the obtained data from the 'Troll' and 'Shadow' targets produced comparable results for headings and fabric strengths (Table 8). In contrast to terrestrial aeolian sediments, particles were found to be highly spherical as they did not exceed length-width ratios of 1.7 (Fig. 39, second column). Further selection with a higher minimum length-width ratio amplified the orientation pattern, yet also rapidly reduced the amount of particles for calculating orientation patterns and other sediment properties. Due to the large pixel scale, rose diagrams were made using a length-width ratio larger than 1.1 such that only very spherical particles were excluded. Bimodal frequency distributions of long-axis orientations were detected for all of the three sites (Fig. 39). Based on the calculated tilt of the camera (Table 8) one of the headings was excluded as a possible orientation axis caused by rolling parallel to the strike of the slope (red lines, Fig. 39) and the second orientation heading was inferred as the wind-induced orientation (blue lines, Fig. 39). The wind-induced headings are very comparable for the targets at Home Plate and good agreement was also found for the wind quadrants of the calculated orientations ($x$). A comparison of the preferred orientations was also made with the orientation of aeolian features at the El Dorado and Home Plate sites (Fig. 40). The long-axis orientation of grains in the sediment fabric were found to align well with the directions of other aeolian features. The most notable deviation with local aeolian features was found at the Shadow ripple in El Dorado.

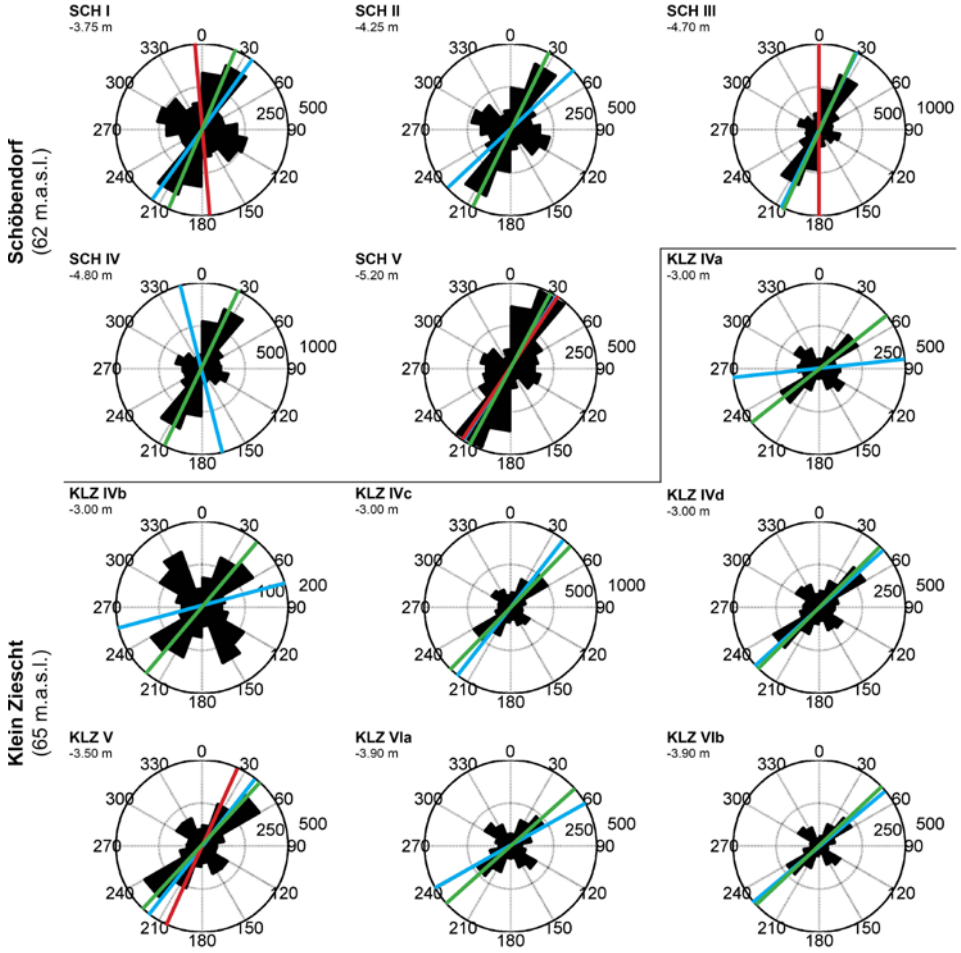


**Fig. 38** - Preferred orientation of grains in thin-sections of aeolian sediment at the Schöbendorf and Klein Zieschт dune complexes. Rose diagrams show the long-axis orientations for all particles with a length-width ratio of >1.5. The average heading relative to true north (x° or x°+180°) is shown for data obtained using video-based analysis (in red), the OBIA method from this study (in blue) and arithmetic means calculated for the preferred orientation (in green). Orientations related to gravity-induced rolling are absent, as thin-sections were made from horizontal laminae. Weak signals in nearly all thin-sections orthogonal to the main heading are examples of wind-induced rolling.

# 5. Discussion

## *5.1 Detecting preferred long-axis orientations in thin-sections*

### *5.1.1 Comparison of the OBIA method with pre-existing techniques*

Relating preferred orientation of grains in thin-sections to local flow conditions is a method that has been around for several decades. Studies by Schwan (1989) and those pre-dating his work relied mostly on the manual extraction of grain properties. Orientations and length-width ratios of quartz grains were therefore estimated by hand using a micro-ruler in the eye-piece of the microscope. These measurements were repeated a minimum of 8 times per grain by rotating the thin-section under crossed polars, until the best measurement was obtained when the grain had the strongest translucence. Improvements using video-based image analysis

**Table 7** - Grain orientations in thin-sections Schöbendorf and Klein Ziescht using particles with a length-width ratio of 1.5 and larger, based on the developed object-based image analysis (OBIA) method and pre-existing video-based image processing (De Boer, 1992). Comparisons can be made between the amount of particles ($n_{>1.5}$), orientation relative to true north ($x$) and the fabric strength ($R$). The latter is a measure of the concentration around the mean orientation ($x$). A value closer to 1 indicates a stronger preferred orientation of grains in the sediment fabric. Other sediment properties include the total amount of detected particles ($n_{tot}$) and the arithmetic mean of the orientation distribution ($x_a$).

| Thin-section | Video-based analysis | | | OBIA using eCognition | | | | |
|---|---|---|---|---|---|---|---|---|
| | $n_{>1.5}$ | $x$ (°) | $R$ | $n_{tot}$ | $n_{>1.5}$ | $x$ (°) | $x_a$ (°) | $R$ |
| Schöbendorf | | | | | | | | |
| *SCH I* | 624 | 175.2 | 0.0864 | 6641 | 2213 | 35.6 | 22.9 | 0.0154 |
| *SCH II* | - | - | - | 5549 | 1914 | 227 | 26.3 | 0.0717 |
| *SCH III* | 760 | 0.1 | 0.1252 | 7348 | 2678 | 26.0 | 24.7 | 0.2425 |
| *SCH IV* | - | - | - | 8900 | 3117 | 166 | 25.6 | 0.1731 |
| *SCH V* | 344 | 33.7 | 0.0561 | 5635 | 1998 | 32.9 | 28.2 | 0.2456 |
| Klein Ziescht | | | | | | | | |
| *KLZ II* | 261 | 126 | 0.0229 | - | - | - | - | - |
| *KLZ IVa* | - | - | - | 3347 | 1224 | 264 | 51.6 | 0.1056 |
| *KLZ IVb* | - | - | - | 2387 | 847 | 75.4 | 40.3 | 0.0837 |
| *KLZ IVc* | - | - | - | 6577 | 2258 | 38.1 | 44.3 | 0.1203 |
| *KLZ IVd* | - | - | - | 3987 | 1333 | 48.0 | 45.0 | 0.0941 |
| *KLZ V* | 232 | 24.5 | 0.0807 | 4815 | 1606 | 38.1 | 42.9 | 0.1650 |
| *KLZ VIa* | - | - | - | 3422 | 1193 | 60.7 | 48.3 | 0.0444 |
| *KLZ VIb* | - | - | - | 2853 | 978 | 50.0 | 46.8 | 0.0844 |

were made possible with equipment such as the Quantimet 970 from Cambridge Instruments (De Boer, 1992). This development reduced potential operator bias as the hardware could automatically detect grains and calculate properties such as area, length, breath (width) and long-axis orientation at pixel resolutions of 1.3 µm. Contrast issues still required the circumference of many grains to be manually traced with an 'image pen' during post-processing steps, if the contrast was insufficient to automatically separate a grain from its surroundings.

Compared to these pre-existing methods, the OBIA method automates the first two steps in a thin-section analysis (grain detections and the quantification of grain properties) and eliminates possible operator bias in these steps and during post-processing of grains. Although the OBIA method still requires some operator intervention to optimise the scale parameter for obtaining satisfactory segmentation and classification results, the quality and quantity of delineating grains are equal if not better than those from other pre-existing methods (e.g. Table 7). Furthermore, the workflow of the OBIA method is much less complex compared to recent GIS-based image processing methods that still rely on the rotation of thin-sections between crossed polars (e.g. Hassanpour, 2011).

Processing of cross-polarised thin-sections is always sensitive to contrast variations that result from the diversity in mineralogical properties (some minerals have a dark colour) and the dependence of grain translucency on the relative orientation between the crossed polars. This is the foremost reason for the inclusion of the rotation stage in pre-existing thin-sections methodologies. The resolving power of the OBIA method at pixel-scales allows such low contrast grains to be detected too, irrespective of their particle diameter. With the

exclusion of thin-section rotation, the OBIA method also cuts down on total processing time with several orders of magnitude (minutes of processing datasets versus days). However, the analysis is based on a rule-set that causes some portion of darker grains not to be detected and classified as they fall outside the specified contrast criteria. Conversely, some irregular shaped objects are erroneously classified as grains due to the low contrast effects. Such artefacts were substantially reduced by including the roundness parameter in the work flow (see Table 6), but a small degree of artefacts is still present in the final classification result. This is illustrated by a closer inspection of Fig. 37. Further refinement of the OBIA method steps is therefore possible, as shown by parameter optimisation in other applications of OBIA strategies (e.g. Anders *et al.*, 2011). Taking these considerations into account, the quantity of detected grains with this method is still much larger and more time-efficient than what can be achieved by hand and eye. The most important prospect of the OBIA method may therefore be this increase in particle detection (several thousand per thin-section), which causes measurements of particle orientations to better reflect the actual state of the sediment fabric. At the same time, large amounts of particles also allow further refinements in the orientation analysis by using different length-width ratios (e.g. 1.0-1.5, 1.5-1.7 or all particles with >1.7) whilst still retaining a statistically sound sample size. This kind of versatility and the level of maturity of multi-resolution segmentation algorithms as implemented in the software suite eCognition (Baatz and Schape, 2000) allow the OBIA method for thin-sections to potentially supersede the analytical performance of other thin-section analysis methods.

### *5.1.2 Relation of detected orientations to wind flow patterns*

The applicability of wind-induced particle orientation data is ultimately determined by how well the measurements made of the sediment fabric relate to (in this case) the local palaeowind directions. In this discussion we will first briefly consider the timing and regional conditions that formed the sampled laminae in Germany to understand how the detected orientations relate to local flow processes at the time of their deposition, and then we will focus on the performance of the OBIA method.

The position of the Schöbendorf and Klein Zieschte dunes in the central Baruth ice-marginal valley relate their maximum TL/OSL ages (16.2±1.9 kyr) to the early formation period of the ice-marginal valley terraces in the Weichselian Lateglacial (Hilgers, 2007). In this period the deposition of initial cover sands was mainly driven by katabatic winds from northerly and easterly quadrants (De Boer, 1992). Thin-sections of the Schöbendorf and Klein Zieschte profiles were sampled from laminated sediments that were part of this initial period of cover sand deposition. While wind regimes driven by oceanic flow patterns from the west are considered to be highly unlikely at this time (Zeeberg, 1998), changes in atmospheric circulation eventually caused a radical shift of dominant winds to westerly and southerly quadrants. This shift is well-reflected by the orientation of the superposed parabolic dunes that post-date the laminae sampled in this study. Rejecting one of the two types of atmospheric flow conditions (katabatic NNE vs. oceanic SSW) is difficult due to the non-vectorial nature of 2D orientation measurements, but we can argue for NNE-winds on the basis of age, climate and proximity of the glacial margin at the time these cover sands were formed. Similar unidirectional katabatic flow patterns have been hypothesised further eastward along the glacial margin on the basis of global circulation models (Zeeberg, 1998).

We used the same thin-sections in this study as in previous studies and the inferred quadrants are in general agreement. However, Fig. 38 and Table 7 also show a 5-28° offset in the average headings ($x$) calculated using video-based and object-based image analyses of the same thin-

sections. This poses the question which of the two methods is correctly reflecting the wind flow conditions. Data obtained with the OBIA method show a very pronounced orientation in both sampled profiles along the azimuth (N)NE-(S)SW, based on 3-6 times the amount of sand grains than those in the study by De Boer (1992). As the inferred headings are also consistent throughout the depth of the profile and may have benefited from the reduction in operator bias or measurement errors, we consider the observed difference in headings between the methods to be a consequence of the larger sample size. A similar interpretation applies to the generally higher fabric strength (*R*) as the larger quantity of particles also gives a better reflection of this sediment property. The re-analysis of the aeolian sediments at Schöbendorf and Klein Ziescht illustrates that the OBIA method seems to be a valid approach for measuring preferred particle orientation patterns that allows wind flow conditions at the time of sediment deposition to be inferred.

### *5.2 Wind directions at the Martian surface*

Aeolian features and the behaviour of wind-mobilised sediment along Spirit's traverse of the Columbia Hills have been extensively studied by Greeley *et al.* (2008), Sullivan *et al.* (2008) and Thomson *et al.*, (2008). The contextual interpretation of inferred wind directions in our study is therefore largely based on their extensive landscape analyses. The imaged sediments consist of mafic 100-300 µm sands that are common in the Columbia Hills and represent the saltation-capable fraction from the regolith in Gusev crater (Sullivan *et al.*, 2008). Transport of these fine sands occurred initially by sporadic storm events from the NNW and SSE that winnowed the regolith to form the local sand deposits at El Dorado and the ripples and sand drifts at Home Plate. As orientations of aeolian ripples are related to the net transport rate, their orientation can be used to infer the local wind direction (Rubin and Hunter, 1987; Andreotti *et al.*, 2006). Ripples in the Columbia Hills are no exception and were formed primarily by saltation, based on the measured particle diameters in these ripples (see Sullivan *et al.*, 2008 for an authoritative review of particles, particle mobility and the relation to bedforms in this area). As preferred orientations of sand grains are formed principally by saltation, we can validly assume that detected orientations (Fig. 39) are directly associated to saltation and as such local wind flow directions. Wide-spread migration of sand drifts and ripples composed of particles similar to the imaged grains in this study was observed during sol 1260-1265 when a storm swept the area around Home Plate and caused up to 2 cm down-wind displacement (Sullivan *et al.*, 2008). Unfortunately, damage was sustained to the optics of the MI during this storm event, hampering the application of the developed OBIA strategy to images postdating the storm. Only images were used that pre-date this event. The orientations detected in the sediment fabric therefore reflect the most recent high-energy wind event, probably related to the storm on sol 417-420. This event mobilised sands and trapped particles on the rover deck before it entered the Columbia Hills (Sullivan *et al.*, 2008). Local wind flow patterns were inferred by Greeley *et al.* (2008) and Thomson *et al.* (2008) by combining surface observations of Spirit's cameras with high-resolution orbital footage of oriented aeolian features. Their analyses focussed on wind-blown ripples and dunes, ventifacts formed by the scouring action of particle impacts during saltation and wind tails of sand deposited on the lee-side of flow obstacles. We have therefore compared the dominant long-axis orientation of particles to this very detailed set of observations of near-surface wind directions along Spirit's traverse of the Columbia Hills.

Imaged particles along the traverse are generally well-rounded, as shown by the length-width ratios in Fig. 39. A benefit of the OBIA method is that grain orientations can be

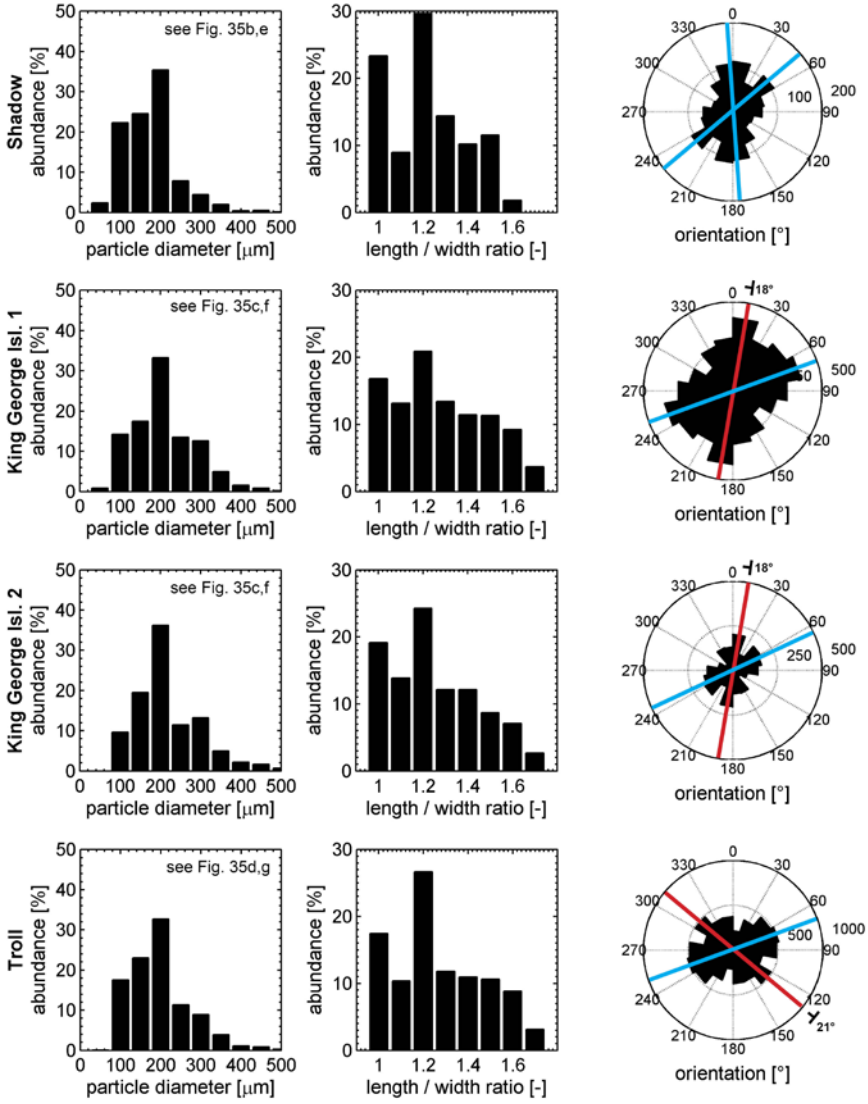


**Fig. 39** - Overview of measured sediment properties on Mars. The first and second columns show the particle size distributions and the length-width ratios. Rose diagrams in the third column show the preferred long-axis orientation of particles with a length-width ratio larger than 1.1. Red lines identify the heading from probable rolling and avalanching of particles down-slope (based on the tilt of the image); blue lines are inferred as the A-axis orientations and reflect the heading of local wind flow. The different orientation of the red line at Troll orthogonal to that of King George Island may indicate an avalanche orientation, considering the same orientation of the dunes.

quantified for very low length-width ratios and this makes the method well-suited to analyse imagery of such aeolian grains. Compared to the studied horizontal laminae of terrestrial covers sands, the analysis of orientations patterns in ripples on Mars is more complicated. Sediments fabrics at all three surface targets were found to exhibit a moderately bimodal 'x-type' pattern where the two headings are not oriented perfectly orthogonal to each other. This rules out that both were formed by wind flow, as identified in some of the terrestrial

**Table 8** - Overview of the orientation data derived from the MI images of sediments on Mars. The image orientation was derived by multiplying the pointing vector of the camera with the quaternion of each image. The obtained orientation in x, y, z was then decomposed into the azimuth and tilt. The number of particles (*n*), orientation relative to true north (*x*° or *x*°+180°) and fabric strength (*R*) of the sediment were then calculated for particles with a length-width ratio larger than 1.1.

| Location | Sol | Image orientation | | | | | Sediment properties | | |
|---|---|---|---|---|---|---|---|---|---|
| | | *x* | *y* | *z* | Azimuth (°)[a] | Tilt (°)[b] | *n* | *x* (°) | *R* |
| El Dorado | | | | | | | | | |
| *Shadow* | 707 | 0.24501 | 0.96923 | 0.02366 | 75.8 | 1.4 | 714 | 356 | 0.1717 |
| Home Plate | | | | | | | | | |
| *King George Isl. 1* | 1034 | 0.14423 | 0.93840 | 0.31401 | 81.3 | 18.3 | 2820 | 359 | 0.1289 |
| *King George Isl. 2* | 1034 | 0.18342 | 0.93164 | 0.31369 | 78.9 | 18.3 | 1194 | 359 | 0.1585 |
| *Troll* | 1058 | 0.49406 | 0.79336 | 0.35565 | 58.1 | 20.8 | 3662 | 28 | 0.1061 |

[a] *azimuth is calculated using atan2(y,x)*

[b] *tilt is calculated using atan2(z,$(x^2+y^2)^{0.5}$)*

laminae (Fig. 38). Dapples and Rominger (1945) showed that when multiple particles are involved in a granular avalanche, their long-axis orientation traverses towards the sediment source, while down-slope rolling of individual particles produces orientations orthogonal to the avalanche direction. The highest slope angles of the stoss sides of ripples and the angles of repose of sand drifts in the Columbia Hills vary between 19-36° (Sullivan *et al.*, 2008). One of the detected headings was interpreted and excluded using the image tilt (Table 8) as a possible preferred orientation related to rolling or avalanching down-slope (red lines in Fig. 39). This non-aeolian rolling interpretation is further supported by the deviating azimuth of these headings with local aeolian features (e.g. Thomson *et al.*, 2008). The other heading was therefore interpreted as an A-axis orientation caused by airborne streamlining during saltation (blue lines in Fig. 39). These headings are in excellent agreement with flow directions reflected by other aeolian processes in the area (Fig. 40). The fabric of aeolian sediments on Mars may thus harbour valuable information on the up-wind source of these sediments after their deposition.

At El Dorado the interpretation of wind flow patterns is more complicated than at Home Plate due to the sinuous nature of ripples at the edge of this contiguous sand deposit (Fig. 36b). Asymmetry of the cross-sectional profile of the largest ($T_1$) ripples show that these bedforms were likely formed by regional winds from the WSW (Sullivan *et al.*, 2008). In this case $T_n$ is the classification used for the largest bedform, with $T_{n+1}$ being a superposed bedform (Warren and Kay, 1987). Smaller $T_2$ ripples with wavelengths of 10 cm are formed inside the 2-3 m wide troughs, often at right angles to the trough axis and interwoven with subtle $T_3$ ripples consisting of fine dust (Sullivan *et al.*, 2008). The orientation of the $T_2$ ripples indicates that wind directions inside the troughs are approximately NNW-SSE oriented, although it should be noted that these flow directions can be highly variable due to the discontinuity of the $T_1$ ripples in the area visited by Spirit. Flow-modification resulting from the ripple topography is known to produce radically different flow patterns in the troughs of ripples (Bourke *et al.*, 2004). These flow modification processes have also been proposed for the orientation of other bedforms in the Columbia Hills by Thomson *et al.* (2008). As the low tilt of the MI camera indicates a low gradient of the surface (Table 8), it eliminates a clear gravity-induced rolling direction in this part of the trough area (Fig. 36b) and bimodal orientation pattern therefore seem to have an aeolian origin. As imagery of Shadow was taken from a $T_2$ ripple, there

can be two hypotheses for the headings along NNW-SSE and ENE-WSW; (1.) the bimodal orientation result from the same wind flow were the orientation pattern is a blend of saltation in bedform-modified winds and the unmodified flow; or (2.) a portion of the particles has been mobilised by a different mode of transport such as rolling, which (partly) oriented the axis to the ENE-WSW heading. Bimodal distributions may indicate two wind regimes at the time of deposition. However, hypothesis 1 is inherently complex and seems to be rejected by the orientation of secondary ripples that clearly reflect the net-transport direction of bedform-modified winds inside the troughs (Sullivan *et al.*, 2008). It is not unlikely that the bimodal orientation pattern was formed only by this bedform-modified flow when considering that different modes of particle transport are possible. Wind tunnel simulations have shown that sand-sized particles >100 µm can indeed be detached and transported by rolling, which can take place at lower wind speeds than what would be required for saltation at the fluid threshold (Merrison *et al.*, 2007). Rolling of particles may also be promoted by the thick laminar sublayer on Mars that engulfs sand-sized particles and to some extent prevents saltation transport (Greeley, 2002; Kok *et al.*, 2012). It is therefore conceivable that some degree of the observed orientation at El Dorado reflects particle mobility at sub-threshold conditions due to the complex interaction of wind flow with the bed. No extensive imaging campaign of other undisturbed sediments at El Dorado was undertaken that would allow us to decisively prove or disprove this interpretation, but it defines a topic that may require further scrutiny by surface investigations elsewhere on Mars or by wind tunnel simulations to understand this type of aeolian behaviour.

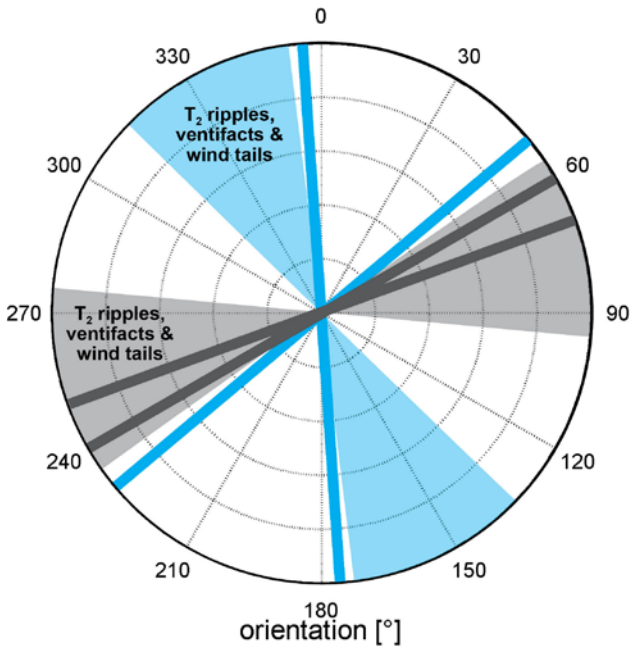


**Fig. 40** - Rose diagram summarising wind directions in the Columbia Hills. Sectors with solid colours are wind directions inferred from ventifacts, wind tails and 2nd-order bedforms ($T_2$) from photographic interpretation of these aeolian features by Greeley *et al.* (2008) and Thomson *et al.* (2008). Solid lines are the preferred orientations of particles measured in the sediment fabric of the three surface targets in this study. Blue sectors and lines correspond to El Dorado; those in grey give the headings for Home Plate.

### *5.3 Saltation conditions, implications and outlook*

Saltation of sands on Mars is one of the most elusive surface processes as atmospheric conditions seem unfit to achieve favourable conditions for this process, in spite of the abundant geomorphic evidence showing that saltation takes place. It has been proposed by Sullivan *et al.* (2008) that the mobilisation of sands in the Columbia Hills is highly dependent on the complex interaction of infrequent storm events with the local topography, rather than the persistent seasonal variations in wind flow suggested by Greeley *et al.* (2008). The formation of aeolian features in the Columbia Hills by high-energy wind events is further evidenced by the observed A-axis orientation in the sediment fabric that only results from airborne streamlining during saltation. Although these wind flow conditions occur sporadic on Mars, several authors have argued that GCM models are unable to resolve the much higher wind speeds at smaller local scales due to the low resolution of these models (Fenton and Michaels, 2010; Kok *et al.*, 2012). Process simulations at much finer scales have recently shown that saltation at the dynamic threshold can indeed be sustained by splashing (reptation) of particles at much lower wind speeds that occur more commonly on Mars than infrequent storm events (e.g. Kok, 2010a, 2010b; Kok *et al.*, 2012). Gusts or topographic forcing of the wind flow can therefore provide the initial 'push' at fluid threshold conditions to set particles in motion, leading to the high rates of observed bedform migration (e.g. Bridges *et al.* 2012a; 2012b) and the preferred orientation of particles in the sediment fabric. Interestingly, these preferred orientations can potentially contribute to wind-induced particle mobility. Once an elongated particle has obtained a preferred (flow-induced) orientation, often with a negative angle of attack dipping into the sediment fabric, the increase in aeolian drag and lift create a resultant force from below the particle that can cause it to flip upward, detach and migrate downwind (Rusnak, 1957). When saltation is achieved, the low air density and gravity causes saltating particles to hop higher and farther down-wind compared to Earth and this leads to a much larger acceleration of the particle (Kok *et al.*, 2012). The range in fabric strengths on Mars (0.1-0.17) varies somewhat compared to Earth (0.01-0.24). Lower fabric strengths of aeolian sediment on Mars may be a likely consequence of the much higher impact velocities of saltating grains that result from this airborne acceleration (Greeley, 2002; Almeida *et al.*, 2008). The disruption of the sediment fabric by particle impacts and the reptation (splashing) of nearby grains therefore causes a much larger loss of preferred orientation compared to Earth. This in turn causes a higher randomisation in long-axis orientation and produces an even larger difference in the fabric strength compared to those of well-oriented fluvial sediments (Rusnak, 1957; Schwan, 1989). The degree of particle orientation in lithified sedimentary facies can thus be used as a powerful tool to discriminate between wet or dry formative conditions of sedimentary rocks on Mars.

We have focused in this study primarily on the 'qualitative' aspects of wind-induced orientation of particles on Mars. Object-based analyses of sediment images on Mars is still in its infancy, but for the application of measuring long-axis grain orientation it has great potential for aeolian surface studies. Measurements of wind speeds in combination with imaging provide further information on the near-surface flow conditions, perhaps even allowing grains to be used as passive flow indicators on multi-sol research stations. While the MER rover Spirit did not have any meteorological instrumentation, the Mars Science Laboratory rover 'Curiosity' is equipped with an environmental sensor suite (Gómez-Elvira *et al.*, 2012) that can be used to correlate *in situ* measurements of wind speeds and directions with observations of grains using the Mars Hand Lens Imager (MAHLI) (Edgett *et al.*, 2012). The developed OBIA method was based on the use of monochromatic imagery of the Microscope

Imager. A benefit of the panchromatic MAHLI camera over the MI camera is the smaller pixel scale of 14 μm and availability of colour channels that increase the information available for the OBIA algorithm, allowing more accurate detection and extraction of aeolian grains from the imagery. Measuring wind flow directions using the sediment fabric can therefore give additional insights in particle mobility on more common diurnal or seasonal scales and during sporadic storm events.

## 6. Conclusions

The orientation of aeolian grains in the fabric of sedimentary facies provides information on local near-surface wind flow directions, independent of profile depth or degree of consolidation. The developed Object-based Image Analysis (OBIA) method shows that sediment statistics such as particle size distributions, particle orientations and fabric strength can be obtained irrespective of the type of sand grain imagery by adapting the criteria of the OBIA strategy. This allows a rapid detection of large quantity of grains in traditional analyses of thin-sections under crossed polars and it improves the accuracy for inferring palaeowind directions. Our analyses have been based on a limited amount of thin-sections and further work is needed to underpin the applicability of this very promising technique in local and regional wind flow reconstructions. The same OBIA strategy can be applied to extreme-close up imagery of sand grains on Mars, providing a similar granulometric analysis of aeolian sediment such as with well-established methods that are based on the analysis of thin-sections. Mars lander and rover cameras with pixel-resolutions of several tens of micrometres therefore provide sufficient image data to allow the detection of preferred grain orientations and infer the directions of the most recent high-energy wind flow event. Particle orientation on Mars occurs mainly in non-cohesive aeolian deposits that consist of well-rounded sand grains, winnowed from fine dust. A much larger fraction of preferred long-axis orientations on Mars can be caused by gravity and wind-induced rolling compared to the portion oriented by saltation in local winds on Earth. Contextual analyses of surficial sediments therefore provide insights in the characteristics and types of particle mobility. With the present focus of lander instrumentation on the geochemical characterisation of surface materials, the method also allows the characterisation of physical particle properties of Martian soils. Ultimately, this form of *in situ* analysis of local wind flow can be a valuable new resource to surface studies of aeolian features on Mars.